ELSEVIER

Full Length Article

Short-term pharmacologic RAGE inhibition differentially affects bone and skeletal muscle in middle-aged mice

Hannah M. Davis[a,b], Alyson L. Essex[a,b], Sinai Valdez[a], Padmini J. Deosthale[a,b],
Mohammad W. Aref[a,b], Matthew R. Allen[a,b,d], Andrea Bonetto[a,b,c], Lilian I. Plotkin[a,b,d,*]

[a] Department of Anatomy & Cell Biology, Indiana University School of Medicine, Indianapolis, IN, United States of America
[b] Indiana Center for Musculoskeletal Health, Indianapolis, IN, United States of America
[c] Department of Surgery, Indiana University School of Medicine, Indianapolis, IN, United States of America
[d] Roudebush Veterans Administration Medical Center, Indianapolis, IN, United States of America

ABSTRACT

Loss of bone and muscle mass are two major clinical complications among the growing list of chronic diseases that primarily affect elderly individuals. Persistent low-grade inflammation, one of the major drivers of aging, is also associated with both bone and muscle dysfunction in aging. Particularly, chronic activation of the receptor for advanced glycation end products (RAGE) and elevated levels of its ligands high mobility group box 1 (HMGB1), AGEs, S100 proteins and Aβ fibrils have been linked to bone and muscle loss in various pathologies. Further, genetic or pharmacologic RAGE inhibition has been shown to preserve both bone and muscle mass. However, whether short-term pharmacologic RAGE inhibition can prevent early bone and muscle loss in aging is unknown. To address this question, we treated young (4-mo) and middle-aged (15-mo) C57BL/6 female mice with vehicle or Azeliragon, a small-molecule RAGE inhibitor initially developed to treat Alzheimer's disease. Azeliragon did not prevent the aging-induced alterations in bone geometry or mechanics, likely due to its differential effects [direct vs. indirect] on bone cell viability/function. On the other hand, Azeliragon attenuated the aging-related body composition changes [fat and lean mass] and reversed the skeletal muscle alterations induced with aging. Interestingly, while Azeliragon induced similar metabolic changes in bone and skeletal muscle, aging differentially altered the expression of genes associated with glucose uptake/metabolism in these two tissues, highlighting a potential explanation for the differential effects of Azeliragon on bone and skeletal muscle in middle-aged mice. Overall, our findings suggest that while short-term pharmacologic RAGE inhibition did not protect against early aging-induced bone alterations, it prevented against the early effects of aging in skeletal muscle.

1. Introduction

Due to the drastic advances in healthcare over the last several decades, people are now living longer than ever before. Paradoxically, this has created a new clinical challenge, i.e. a vast array of chronic degenerative diseases, including heart disease, cancer, diabetes, neurodegeneration, often accompanied by the development of debilitating conditions, such as sarcopenia and osteoporosis [1–3]. To combat these pathologies of aging, there has been growing interest in geroscience, a research field focused on identifying/targeting common biological mechanisms that drive aging and underlie aging-related pathologies [1,4]. Recent advancements in this field have identified several

common key risk factors, such as chronic-low grade inflammation, cellular senescence, metabolic dysfunction, macromolecular damage, genomic instability, reduced responsiveness to stress and altered proteostasis, associated with numerous of these 'comorbidities of aging' [2–6].

However, to date, most work has focused primarily on the mechanisms underlying cardiovascular disease, cancer and neurodegeneration; whereas, the mechanisms underlying debilitating aging-related conditions, such as sarcopenia and osteoporosis, have been less studied. Given the skyrocketing number of individuals with osteoporosis [affecting ~1:2 women of all ages, and ~1:4 men over age 50 and costing the US ~$25.3 billion a year in healthcare expenses [7,8]] and the

increasing incidence of sarcopenia [affecting ~13% of Americans over age 55 and costing the US ~\$18.5 billion a year in related-health expenses [9,10]], there is an essential need to better understand the mechanisms leading to musculoskeletal pathology.

Further, considering the growing evidence showing the interconnected relationship between bone and skeletal muscle [11–13], and the fact that most elderly patients with bone and muscle loss are also affected by other aging-related comorbidities [1,14], there is a crucial need to identify therapeutics capable of simultaneously targeting and treating multiple pathologies.

Low-grade chronic inflammation is one factor identified as a key driver of numerous aging-related pathologies [15,16]. Various cell types release inflammatory cytokines, which not only regulate immune response, but also modulate key cellular processes: differentiation, proliferation, apoptosis, and autophagy throughout the organism [15–17]. In particular, emerging evidence suggests that inflammatory cytokine signaling plays a role in regulating bone and skeletal muscle metabolism under both physiological and pathological conditions [18,19]. Consistently, chronic low-grade inflammation has been identified as a major contributor of dysfunction in both musculoskeletal tissues in aging [20–22].

Particularly, elevated RAGE [receptor for advanced glycation end-products] signaling has been shown to contribute to the onset/progression of various aging-related pathologies [16,23]. RAGE is a multi-ligand pattern recognition receptor, which binds and mediates the cellular response to a range of endogenous damage-associated molecular pattern molecules (DAMPs) including advance glycation end-products (AGEs), high mobility group box 1 (HMGB1), S100 proteins, Aβ fibrils, and DNA/RNA [24,25]. Under physiological conditions, RAGE is expressed at low levels, but during conditions of chronic inflammation RAGE is upregulated due to the accumulation of its ligands [16,25].

Numerous studies have demonstrated beneficial effects with RAGE inhibition [genetic and pharmacological] in various aging-related pathologies including diabetes, cardiovascular disease, neurodegeneration, and cancer [26]. Further, downregulation of RAGE signaling has been shown to protect against disease-induced bone and muscle loss. Particularly, in bone, genetic RAGE deficiency prevented against OVX induced bone loss in mice; and consistently, blockade of cellular RAGE using soluble RAGE diminished alveolar bone loss in a murine model of diabetic periodontal disease [27,28]. Additionally, in skeletal muscle, young mice fed a diet high in AGEs exhibited impaired skeletal muscle growth and contractile function [29]. Interestingly, AGEs were found to induce skeletal muscle atrophy by stimulating RAGE-mediated AMPK down-regulation, an effect that was attenuated in RAGE-deficient mice [30]. Moreover, high intracellular levels of RAGE ligand, S100B, known to inhibit myogenic differentiation by repressing the myogenic regulatory factors MyoD and myogenin, were detected in muscle satellite cells isolated from aged subjects [31]. Taken together, these pieces of evidence highlight the potential involvement and the therapeutic opportunity to target/inhibit RAGE signaling during the onset/progression of bone and muscle pathology in aging.

Small-molecule RAGE inhibitors have been developed and their therapeutic utility has been evaluated in pre-clinical and clinical studies over the last decade [32]. For example, TTP488 (Azeliragon, AZ), a small-molecule compound that prevents RAGE from binding to AGEs, HMGB1, S100 proteins, and Aβ fibrils (Fig. 1A), has been evaluated for the treatment of Alzheimer's disease in pre-clinical and clinical studies ([33,34,78]). However, whether pharmacological inhibition of RAGE affects bone and muscle in young individuals, and whether it attenuates the loss of bone and muscle mass in aging is not known. In this study we examined the possibility of repurposing the Alzheimer's drug, AZ, to prevent aging-induced osteoporosis and sarcopenia. Here we report that while RAGE inhibition does not attenuate the effects of aging on bone, it mitigates the effects of aging on skeletal muscle.

2. Results

2.1. AZ differentially alters bone metabolism through direct and indirect actions

To test the effects of pharmacological RAGE inhibition using the small-molecule inhibitor, AZ (Fig. 1A), on osteoclast differentiation, we first treated wildtype non-adherent bone marrow cells (BMC) isolated from 4-month-old (young) or 16-month-old (middle-aged) C57BL/6 female mice (NIH/NIA [35]) with vehicle (veh) or AZ *in vitro*. Consistent with previous findings in global genetic RAGE knockout mice [36], a lower number of mature osteoclasts (≥ 3 nuclei) developed from young or middle-aged BMCs treated with AZ (Fig. 1B). Further, more osteoclast were developed when cells were isolated from middle-aged mice. Based on these findings, we next investigated the *in vivo* effects of systemic AZ administration on osteoclast differentiation/activity and whether it prevents bone loss in early aging. To this end we treated female wild type C57BL/6 4-month-old (young) and 15-month-old (middle-aged) mice daily with AZ (~4 μg/g) or veh for 28 days (Fig. 2A).

Bone histomorphometric analysis of veh-treated mice revealed no alterations in osteoclast number (N.Oc/BS) or surface (Oc.S/BS) per bone surface on the femur endocortical or vertebral cancellous bone surfaces (Fig. 2B,C) with aging, although, vertebral cancellous osteoclast number per tissue area (N.Oc/T.Ar) was lower in middle-aged compared to young veh-treated mice. Further, vertebral cancellous bone perimeter (B.Pm) was decreased in the middle-aged compared to young mice (Fig. 2C). Vertebral cancellous osteoclast number per tissue area (N.Oc/T.Ar) was lower in middle-aged compared to young veh-treated mice. Consistently, osteoclast gene expression was significantly decreased (Fig. 2D) and serum bone resorption marker, C-terminal telopeptide (CTX), levels were lower in middle-aged compared to young veh-treated mice (Fig. S1).

Consistent with the *in vitro* findings, static histomorphometric analysis revealed that AZ treatment in young and middle-aged mice significantly reduced the number of osteoclasts on the vertebral cancellous and femoral cortical bone surfaces (Fig. 2B,C). However, the decreased vertebral osteoclast parameters appear to be a result of increases in vertebral cancellous B.Pm, rather than decreases in N.Oc/BS or Oc.S/BS since N.Oc was not changed in the AZ-treated mice (Fig. 2C). Likewise, AZ treatment did not alter the expression of any osteoclast-related genes in the tibia, aside from an increase in calcitonin receptor (Fig. 2D). Further, we were surprised to find that serum CTX levels were higher in the AZ-treated mice at both ages (Fig. S1), suggesting that more bone surfaces are being resorbed in the presence of AZ.

We next examined the effects of aging and AZ treatment on osteoblast differentiation and function. Histomorphometric analysis revealed that vertebral cancellous osteoblast number per tissue area (N.Ob/T.Ar) was significantly decreased in middle-aged compared to young veh-treated mice. However, because vertebral cancellous B.Pm was decreased in the middle-aged mice, osteoblast number and surface per bone surface (N.Ob/BS and Ob.S/BS) were unchanged (Fig. 3A). Further, veh-treated middle-aged mice exhibited lower serum bone formation marker, pro-collagen type 1 N-terminal propeptide (P1NP) levels (Fig. 3B), and gene expression analysis detected similar decreases in mRNA levels for osteoblastic genes with aging (Fig. 3C). However, no aging-related changes in mineral apposition rate (MAR), mineralizing surface (MS)/BS, or bone formation rate (BFR)/BS were detected by dynamic histomorphometric analysis of the vertebral cancellous bone of young and middle-aged veh-treated mice (Fig. 3D). On the other hand, age-related alterations in bone formation were detected on the surfaces of the femur mid-diaphysis (Fig. 3E), suggesting that in the middle-aged veh-treated control mice only cortical bone formation was altered.

In contrast to the effects of AZ on osteoclasts, the effects on osteoblasts were age-dependent. Specifically, while vertebral cancellous
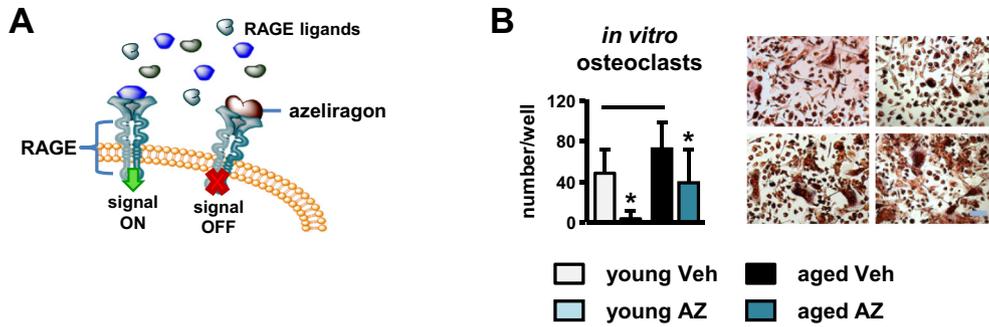
Fig. 1. AZ suppresses osteoclast differentiation in vitro. A) Illustration of AZ mechanism of action. B) Mature osteoclasts/well generated in vitro from non-adherent BMCs from young and middle-aged WT female mice (*n* = 6). Representative images are shown, scale bar indicates 50 μm.
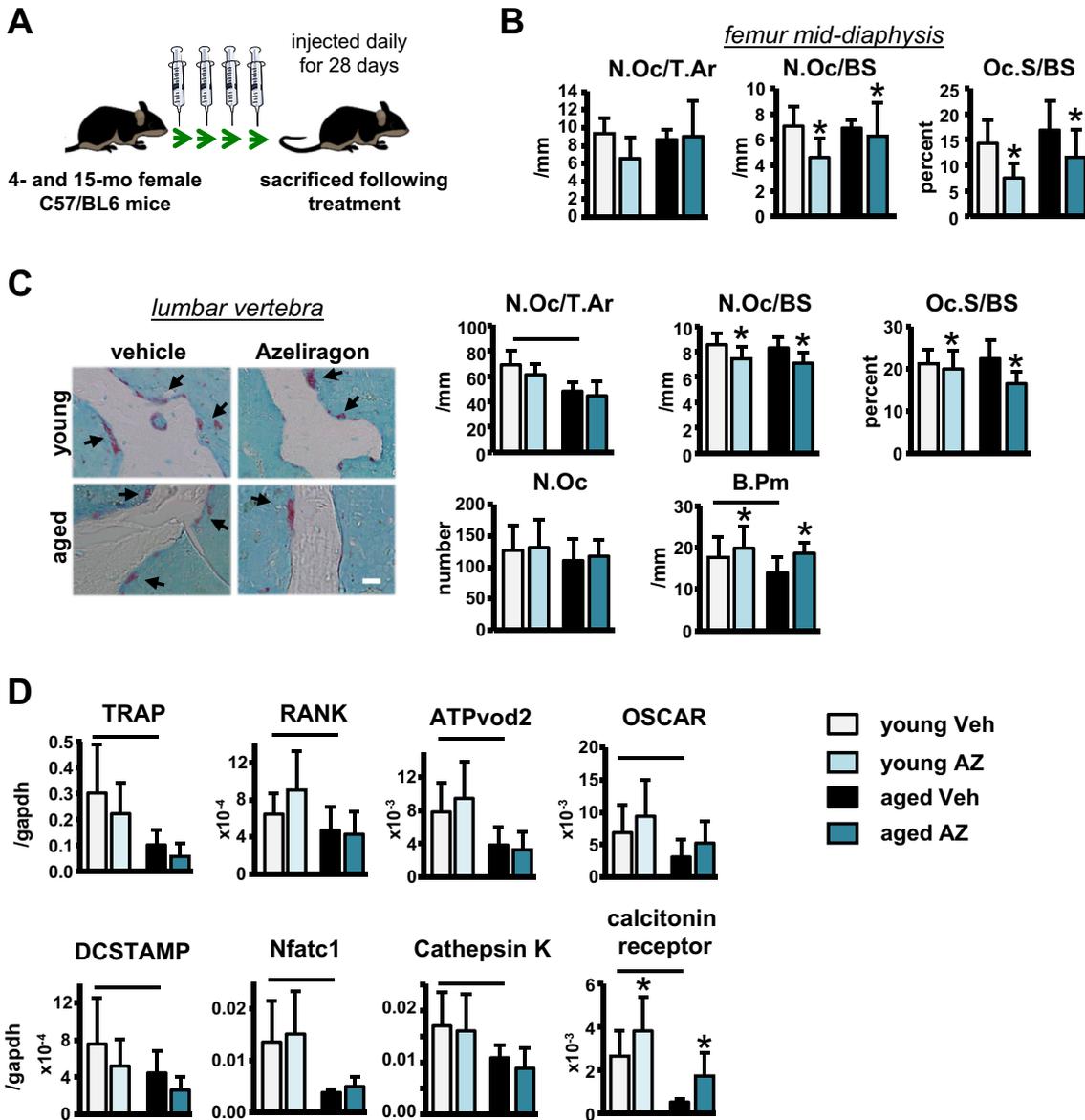

Fig. 2. Short-term AZ treatment has modest effects on osteoclasts in vivo. A) Illustration of in vivo experimental design. Osteoclasts on B) femoral cortical mid-diaphysis and C) vertebral cancellous TRAP/T.blue stained sections (*n* = 8–9). Representative images are shown (black arrows point at osteoclasts), scale bar indicates 25 μm. D) Osteoclast-related gene mRNA expression in whole tibia samples isolated from young and aged vehicle- and Azeliragon-treated mice (n = 8–10). Bars represent mean ± SD, black line: p < 0.05, for the overall age effect and *p < 0.05, vs veh-treated mice at the same age by two-way ANOVA, Tukey.

osteoblast parameters, N.Ob/T.Ar, N.Ob/BS and Ob.S/BS were lower with AZ treatment in mice at both ages, uncorrected N.Ob was only lower in the middle-aged AZ-treated mice (Fig. 3A). Consistently,

dynamic histomorphometric analysis only detected decreases in bone formation in the vertebral cancellous and femur mid-diaphysis en-docortical bone in the middle-aged, but not young AZ-treated mice
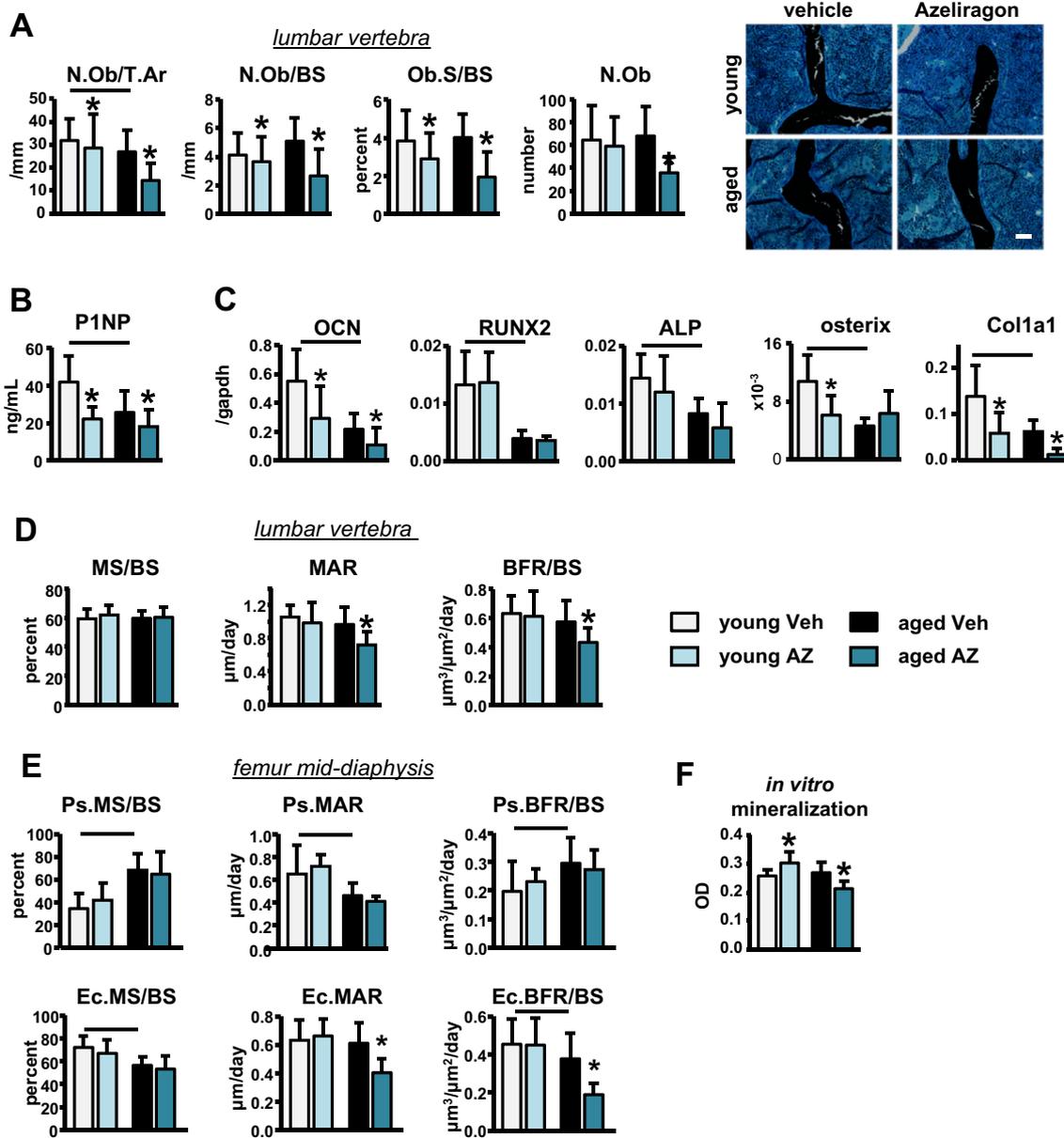
Fig. 3. Short-term AZ treatment attenuates osteoblast differentiation/activity in vivo. A) Osteoblasts on von Kossa/McNeal stained vertebra sections (n = 7–10). Representative images are shown, scale bar indicates 25 μm. B) Circulating serum PINP levels in young and aged veh- and AZ-treated mice (n = 8–10). C) mRNA expression of osteoblast-related genes in whole tibia samples isolated from young and aged vehicle- and Azeliragon-treated mice(n = 8–10). D) Dynamic histomorphometric parameters in unstained vertebra sections (n = 8–10). E) Mineral apposition rate (MAR), mineralizing surface (MS)/BS, and bone formation rate (BFR)/BS measured in unstained sections of the femoral mid-diaphysis from young and aged vehicle- and Azeliragon-treated mice (n = 8–10). F) Mineralization assay of primary osteoblasts generated in vitro from adherent-BMCs from young and middle-aged WT mice (*n* = 5). Bars represent mean ± SD, black line: p < 0.05, for the overall age effect and *p < 0.05, vs veh-treated mice at the same age by two-way ANOVA, Tukey.

(Fig. 3D,E). Additionally, in vitro treatment of young and middle-aged primary adherent BMCs had age-dependent effects, increasing mineralization in young cells, but attenuating mineralization in aged cells (Fig. 3F). On the other hand, systemic in vivo AZ treatment decreased serum P1NP levels in both young and aged mice (Fig. 3B). Further, osteoblast gene expression was decreased in the tibia with AZ treatment in both ages (Fig. 3C). Taken together these results suggest that inhibition of RAGE signaling may differentially affect osteoblast differentiation/activity in an age-dependent manner.

2.2. Inhibition of RAGE signaling increases osteocyte apoptosis and pro-inflammatory cytokine production

Based on the notion that osteocytes are key regulators of bone turnover and to the idea that aging-related reductions in osteocyte viability contribute to bone loss [37], we next sought to test the effects of AZ treatment on osteocytes. We first measured osteocyte apoptosis in active capase3-stained femur cortical bone cross-sections. Aging did not alter the proportion of active capase3 positive apoptotic osteocytes, as found before by TUNEL staining [38], but the number of empty lacunae (an indication of dying osteocytes) was increased in middle-aged compared to young veh-treated mice (Fig. 4A). Additionally, osteocyte gene expression was decreased with aging (Fig. 4B), and consistent with the decreased osteoclast parameters observed in the middle-aged mice, RANKL/OPG gene expression was lower in middle-aged mice compared to young animals (Fig. 4C).

AZ treatment did not alter the proportion of active capase3-positive apoptotic osteocytes, but significantly increased empty lacunae
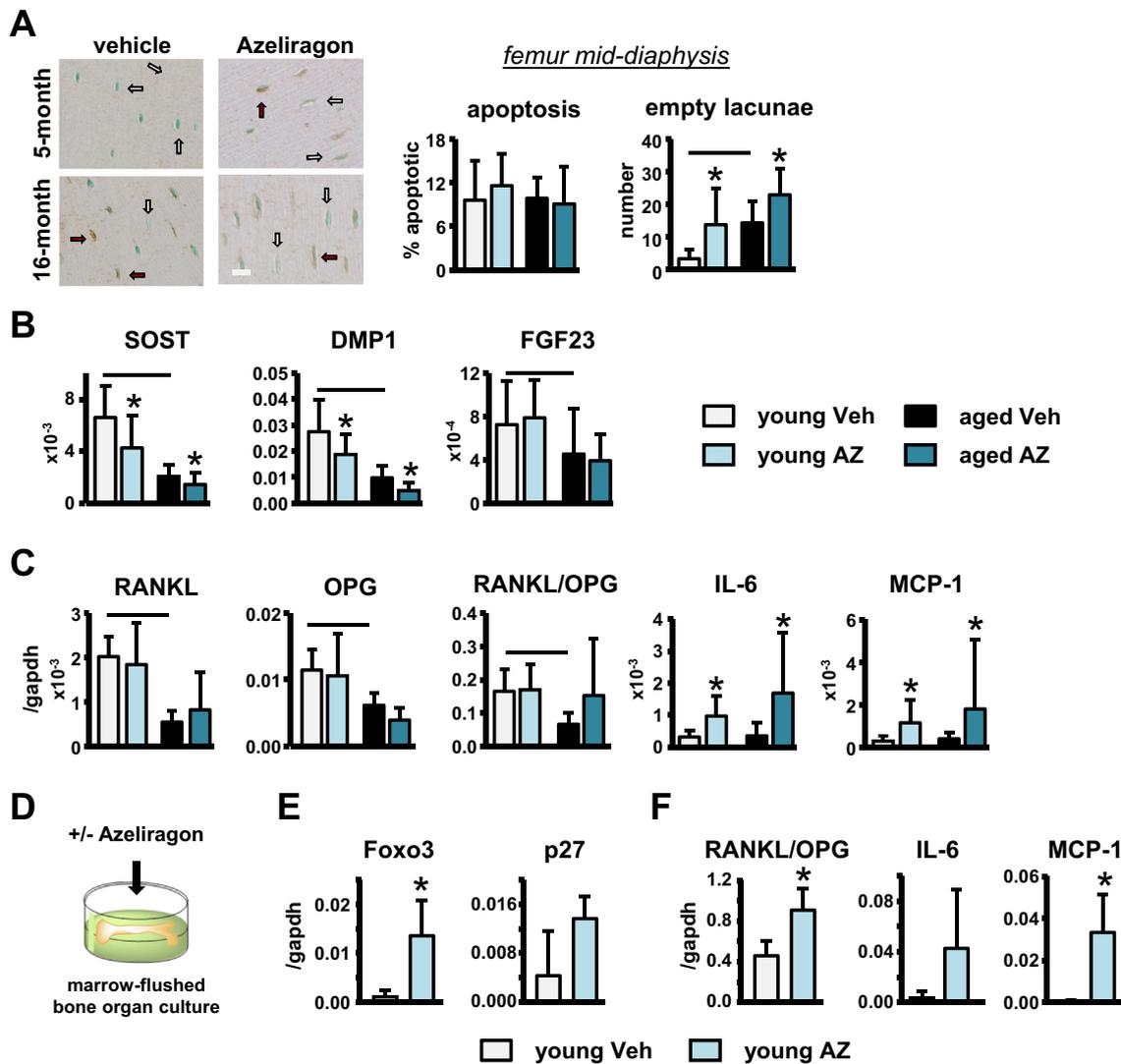
Fig. 4. Systemic RAGE inhibition with AZ treatment increases osteocyte apoptosis and pro-inflammatory cytokine production. A) Active caspase3-positive apoptotic osteocytes and number of empty lacunae scored in active caspase3 stained bone sections (n = 8–10). Representative images of active caspase3-positive osteocytes (arrow, red), scale bar indicates 10 μm. B) Osteocytic gene and C) cytokine mRNA levels in tibia from young and middle-aged veh and AZ-treated mice (n = 7–10). D) Illustration of bone organ culture experimental design. mRNA expression of E) apoptosis-associated and F) pro-inflammatory cytokines in marrow-flushed bone cultures (*n* = 3–5). Bars represent mean ± SD, black line: p < 0.05, for the overall age effect and *p < 0.05, vs veh-treated mice at the same age by two-way ANOVA, Tukey.

prevalence in young and middle-aged mice (Fig. 4A). Consistently, the expression of the osteocyte genes Sost and DMP1 was decreased with AZ treatment in both ages (Fig. 4B), whereas, AZ treatment increased the RANKL/OPG ratio in bones from middle-aged mice and led to higher inflammatory cytokine IL-6 and MCP-1 gene expression in bones from young and middle-aged mice (Fig. 4C). Further, gene expression analysis detected tendencies towards increase in the expression of the apoptosis-associated genes p27 and Foxo3, and a significant increase in the RANKL/OPG mRNA ratio, and in the levels of IL-6 and MCP-1 in *ex vivo* AZ treated osteocyte-enriched bone organ cultures (Fig. 4D–F).

2.3. Short-term systemic RAGE inhibition with AZ treatment does not significantly alter bone architecture or mechanical properties

Dual energy x-ray absorptiometry (DXA) analysis showed that spinal bone mineral density (BMD) was significantly decreased with aging, whereas, total and femoral BMD were unchanged in the middle-aged compared to young veh-treated mice (Fig. 5A). On the other hand, micro-computed tomography (μCT) analysis and 3-point femoral biomechanical testing detected the expected changes in bone geometry

and mechanics, respectively. Specifically, lumbar vertebra and distal femur trabecular BV/TV (bone volume/tissue volume) and trabecular number (Tb.N) were decreased, whereas trabecular spacing (Tb.S) was increased in the middle-aged mice compared to young veh-treated mice (Fig. 5B,C). In addition, femur cortical BA/TA (bone area/tissue area) was decreased, whereas, polar mean moment of inertia (MMI), a measurement of resistance to bending, marrow cavity widening, and bone tissue porosity were increased with aging (Fig. 5D). Further, the biomechanical properties at the structural and material levels were all decreased in the middle-aged compared to young veh-treated mice, with the exception of stiffness, which was increased with aging (Table 1).

Consistent with the changes in bone cell differentiation/activity, DXA analysis revealed that AZ treatment decreased total and femoral BMD in young and middle-aged mice, without affecting spinal BMD (Fig. 5A). However, despite the effects on BMD, no changes in bone geometry (trabecular and cortical) or biomechanical properties following systemic short-term AZ treatment in mice at either age were detected by μCT analysis or 3-point femoral biomechanical testing, respectively (Fig. 5B-D and Table 1).
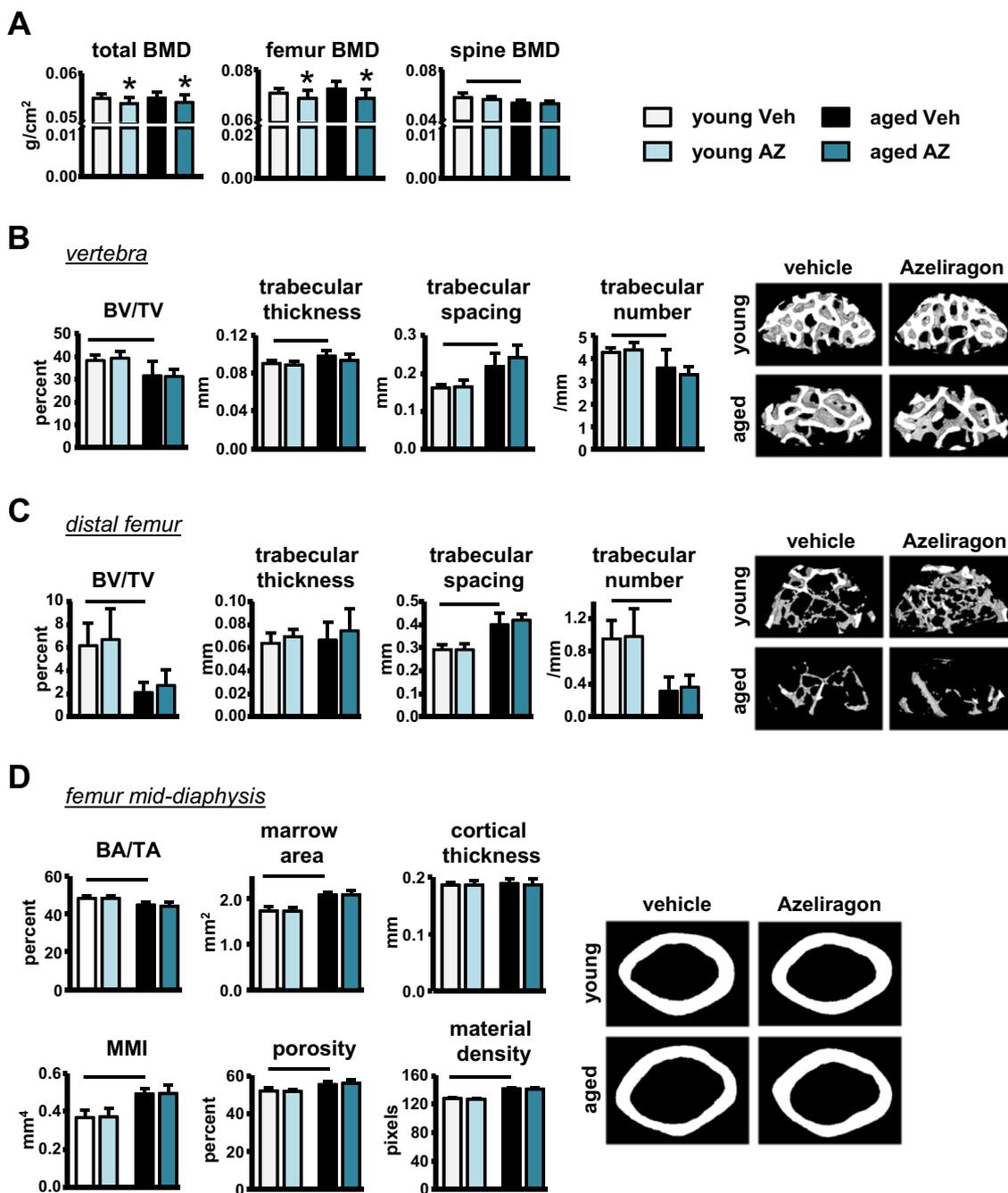
Fig. 5. Short-term AZ treatment decreases bone mass accrual, but not bone architecture in young or old mice. A) BMD of young and middle-aged mice following veh- or AZ-treatment (n = 8–10). Cancellous microarchitecture evaluated by μCT in the B) L4 vertebra and C) distal femur (n = 8–9). Representative images are shown. D) Cortical bone geometry evaluated by μCT in the femoral mid-diaphysis (n = 8–9). Representative images are shown. Bars represent mean ± SD, black line: p < 0.05, for the overall age effect and *p < 0.05, vs veh-treated mice at the same age by two-way ANOVA, Tukey.

2.4. Systemic RAGE inhibition prevents the loss of lean muscle mass and preserves the function of cellular processes required to maintain skeletal muscle homeostasis in aging

Based on the previous reports that both aging and RAGE signaling alter adipose and skeletal muscle mass [29], we next tested the effects of systemic AZ treatment on these tissues. As expected, body weight of middle-aged compared to young veh-treated mice was increased (Fig. 6A), and body composition was altered, with greater fat mass and lower lean mass compared to young veh-treated mice (Fig. 6B). Consistently, gastrocnemius, tibialis anterior, and quadriceps mass corrected by body weight were all decreased in the middle-aged veh-

treated mice (Fig. 6C). Further, gene expression analysis detected decreases in the expression of MyoD with aging (Fig. 6D). Moreover, histomorphometric analysis of H&E-stained forearm skeletal muscle revealed decreases in the average myofiber cross-sectional area (CSA) in middle-aged compared to young veh-treated mice (Fig. 7A,B). Interestingly, *in vitro* treatment of C2C12 myotubes with 5% serum from middle-aged compared to young veh-treated mice also reduced average myotube diameter and led to a shift towards smaller fibers in the representative histograms of the distribution of myotube diameter (Fig. 7C,D), suggesting that circulating serum factors may contribute to aging-induced muscle atrophy. Consistent with the increased muscle atrophy, ubiquitinated protein levels and expression of the E3 ubiquitin

Table 1
Biomechanical properties measured in the femoral mid-diaphysis by 3-point bending test.

	Vehicle 5-month-old	RAGE inhibitor 5-month-old	Vehicle 16-month-old	RAGE inhibitor 16-month-old
Yield force (N)	12.67 ± 2.38	14.81 ± 2.26	9.08 ± 3.37[#]	9.23 ± 4.16
Ultimate force (N)	15.09 ± 0.93	15.70 ± 1.31	16.86 ± 1.52	15.69 ± 2.87
Displacement to yield (μm)	372.58 ± 37.86	419.13 ± 51.66	256.65 ± 122.07[#]	280.42 ± 137.34
Postyield displacement (μm)	642.63 ± 344.32	439.93 ± 147.15	332.56 ± 150.72[#]	394.35 ± 70.29
Total displacement (μm)	991.91 ± 327.71	773.72 ± 172.42	584.99 ± 92.72[#]	633.75 ± 119.06
Stiffness (N/mm)	34.27 ± 3.79	36.11 ± 2.88	44.02 ± 8.09[#]	43.81 ± 7.84
Work to yield (mJ)	2.64 ± 0.76	3.35 ± 0.80	1.47 ± 1.27[#]	1.66 ± 1.25
Postyield work (mJ)	6.85 ± 3.20	5.55 ± 1.48	4.25 ± 1.84[#]	4.56 ± 0.73
Total work (mJ)	9.23 ± 3.19	8.39 ± 2.47	6.16 ± 1.77[#]	5.52 ± 1.26
Yield stress (MPa)	75.51 ± 19.78	71.99 ± 21.16	48.16 ± 18.39[#]	49.46 ± 22.18
Ultimate stress (MPa)	91.83 ± 11.62	86.58 ± 9.87	89.98 ± 10.44	84.14 ± 12.12
Strain to yield (mε)	365.29 ± 56.95	341.73 ± 111.10	307.97 ± 152.87	301.48 ± 147.93
Total strain (mε)	933.81 ± 322.76	713.88 ± 165.82*	630.26 ± 106.21[#]	687.64 ± 113.83
Modulus (GPa)	2.16 ± 0.38	2.12 ± 0.15	2.20 ± 0.34	2.18 ± 0.47
Resilience (MPa)	1.50 ± 0.54	1.69 ± 0.47	0.85 ± 0.75[#]	0.95 ± 0.72
Toughness (MPa)	5.20 ± 2.14	4.03 ± 1.05	3.56 ± 1.10[#]	3.53 ± 1.01

[#] $p < 0.05$ versus treatment-matched young mice.

* $p < 0.05$ versus age-matched vehicle-treated mice, by two-way ANOVA ($n = 7$–9).

ligases Atrogin-1 and MuRF-1, generally overexpressed in conditions associated with muscle atrophy [39,40], were increased in the skeletal muscles of middle-aged compared to young veh-treated mice (Fig. 7E,F).

In young mice, AZ decreased body weight (Fig. 6A), and altered body composition reducing the fat mass and increasing lean mass (Fig. 6B). Consistently, gastrocnemius and tibialis anterior muscle mass (Fig. 6C), as well as myogenin and MyoD expression, measured in the tibialis anterior muscle (Fig. 6D), were increased with AZ treatment. However, quadriceps muscle weight was decreased (Fig. 6C) and the level of ubiquitinated proteins appear to increase with treatment in the young mice (Fig. 7E). Notably, addition of serum from the young AZ-treated mice to C2C12 myotubes also significantly reduced myofiber size and histomorphometric analysis of H&E-stained forearm muscle

revealed decreases in the average myofiber CSA in young AZ-treated mice (Fig. 7B,C).

In middle-aged mice, AZ had similar effects on body composition, reversing the aging-associated increases in body weight (Fig. 6A), as well as, the alterations in body composition by reducing the fat mass and increasing lean mass (Fig. 6B). Further, AZ reversed the aging-induced loss of the gastrocnemius, tibialis anterior, and quadriceps muscle mass in the middle-aged treated mice (Fig. 6C). Consistently, RAGE inhibition increased myogenin expression at both ages, and restored MyoD levels in the middle-aged mice (Fig. 6D). Moreover, while AZ did not completely reverse the aging-induced decreases in myofiber CSA (Fig. 7B), in vitro treatment of C2C12 myoblasts with serum from the middle-aged AZ-treated mice did not result in the decreased myotube diameter that was induced by serum from the middle-aged veh-
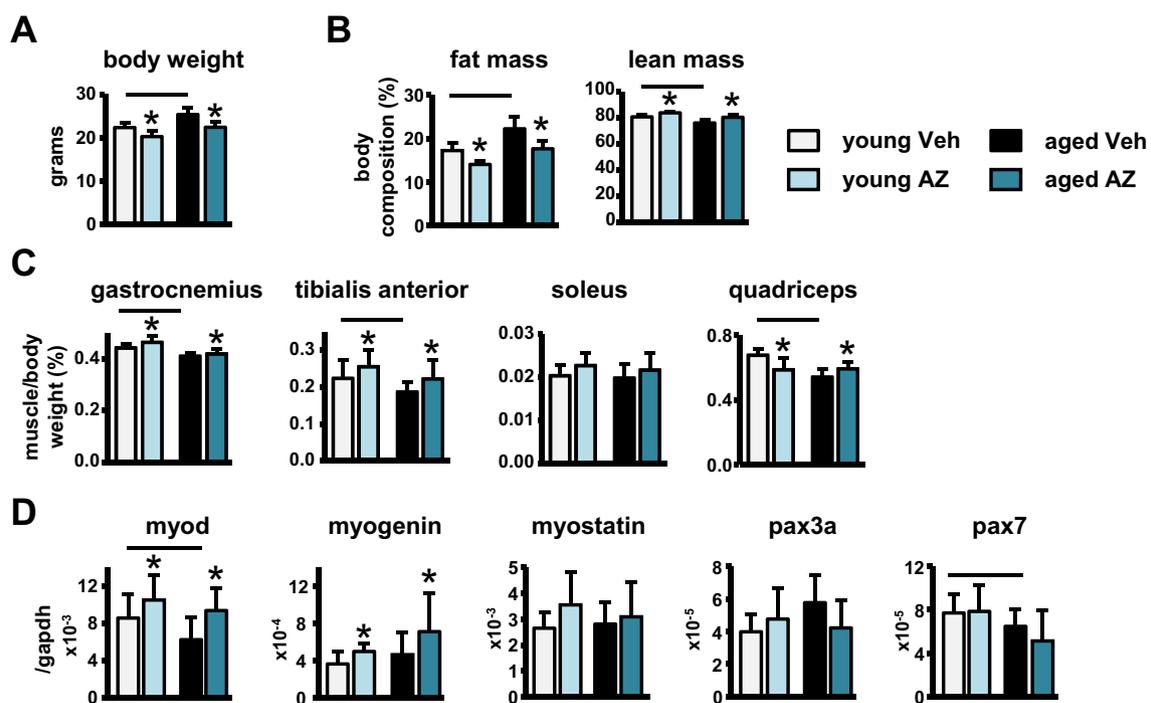

Fig. 6. AZ treatment reverses the loss of skeletal muscle mass induced with aging. A) Body weight, B) fat and lean mass indicated as percentage of body weight ($n = 8$–10), C) muscle weights ($n = 8$–9), D) myogenesis and satellite cell marker mRNA expression in tibialis anterior muscle ($n = 7$–9) of young and middle-aged mice. Bars represent mean ± SD, black line: $p < 0.05$, for the overall age effect and *$p < 0.05$, vs veh-treated mice at the same age by two-way ANOVA, Tukey.
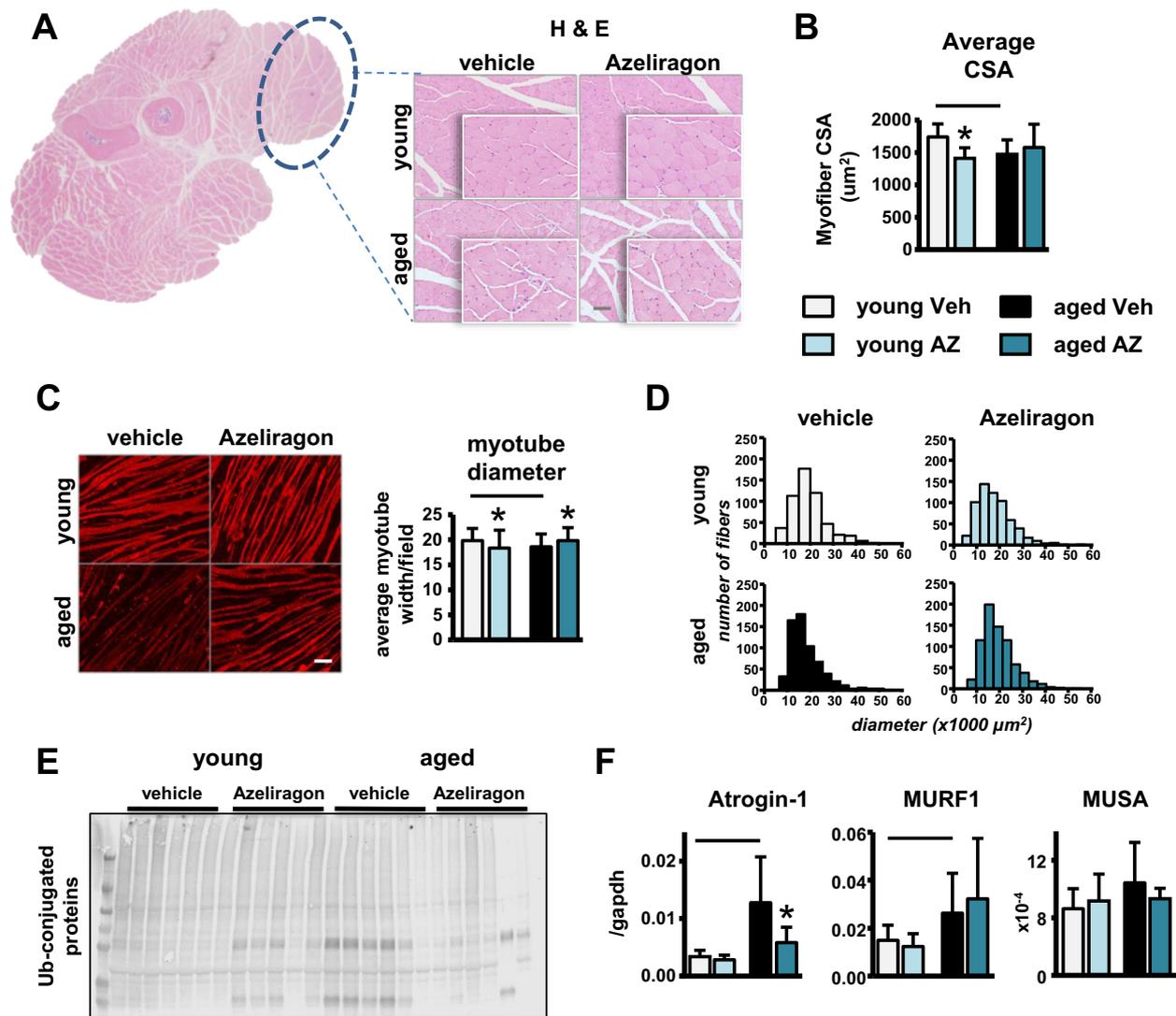
Fig. 7. AZ treatment partially improves the cellular processes involved in maintaining skeletal muscle homeostasis in aging. A) low- and high-magnification images of forearm muscle cross-sections, muscle of interest is circled in black, scale bar indicates 50 μm, and B) average myofiber cross-sectional area (CSA) (n = 6–8). C) Representative images (scale bar indicates 50 μma) and average myotube diameter per field and D) distribution of myotube diameter of serum-treated C2C12 cells (*n* = 10). E) Ubiquitin-conjugated and GAPDH protein patterns in skeletal muscle (n = 6). F) mRNA levels of atrophy-related genes in tibialis anterior muscle (n = 7–9). Bars represent mean ± SD, black line: p < 0.05, for the overall age effect and *p < 0.05, vs veh-treated mice at the same age by two-way ANOVA, Tukey.

treated mice (Fig. 7C,D).

Consistent with these findings, AZ attenuated the aging-induced increases in ubiquitinated protein levels and the mRNA levels of Atrogin-1 (Fig. 7E,F). Further, AZ treatment reversed the aging-associated alterations in the expression of genes involved in the regulation of skeletal muscle cellular processes. Particularly, autophagy- and mitochondria-related gene expression was decreased with aging, and AZ treatment increased expression of these genes in young and middle-aged mice (Fig. S2), suggesting that *in vivo* AZ treatment may protect against aging-induced muscle atrophy, in part, by preserving the proper functioning of cellular processes normally required to maintain skeletal muscle homeostasis and metabolism. On the other hand, while aging increased Atrogin-1 and MuRF-1 levels in bone, as previously shown with glucocorticoid administration [41], AZ did not block these increases (Fig. S3).

2.5. AZ treatment reverses the aging-induced metabolic alterations in skeletal muscle but not in bone

Despite the similar aging-induced loss of bone and muscle mass, the findings from the present study reveal that aging differentially alters skeletal muscle and bone metabolism. Particularly, gene expression analysis of skeletal muscles from young and middle-aged veh-treated mice demonstrated that aging decreased glucose transporter (Glut1-4) gene expression (Fig. 8A). Further, gene expression of glycolytic enzymes (PGK1, LDHA, PDK1) was decreased with aging, whereas the levels of PGC-1α, an enzyme involved in the regulation of oxidative metabolism were unchanged with aging in the veh-treated mice (Fig. 8B,C). In contrast, in bone, Glut3 gene expression was decreased with aging, whereas Glut1 and Glut2 expression was significantly increased and Glut4 was not changed with aging (Fig. 6D). Further, LDHA and PGK1 expression was increased with aging, whereas PGC-1α and PPAR-α expression was unaltered in bone samples from middle-aged compared to young veh-treated mice (Fig. 8E,F).

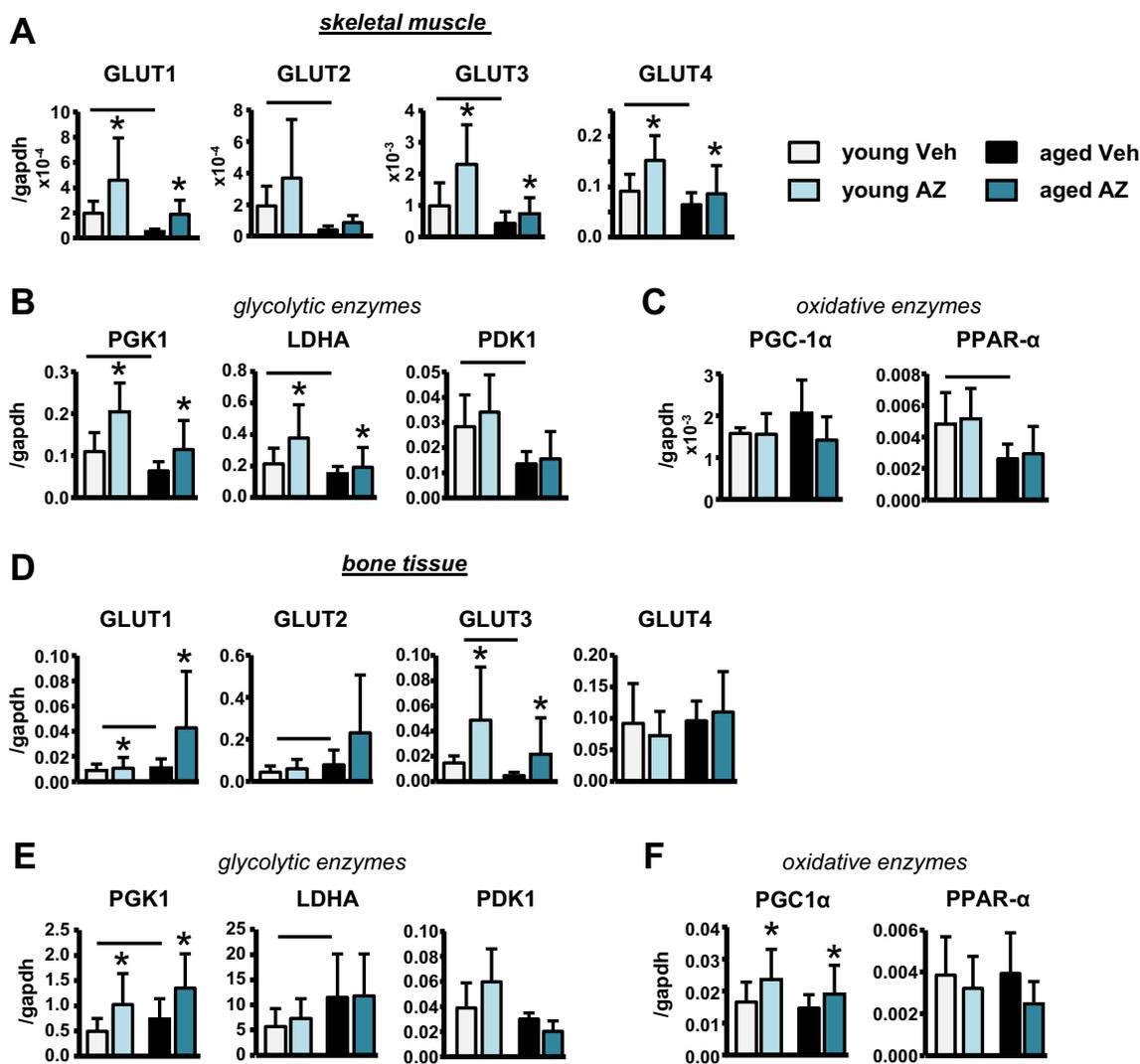We next examined the effects of AZ treatment on the expression of

Fig. 8. Systemic inhibition of RAGE signaling reverses the aging-induced metabolic alterations in skeletal muscle, but not in bone. Glucose transporter GLUT1-4, and glycolytic and oxidative enzyme mRNA levels in tibialis anterior muscle (A–C) and in tibia (D–F) (n = 7–9). Bars represent mean ± SD, black line: p < 0.05, for the overall age effect and *p < 0.05, vs veh-treated mice at the same age by two-way ANOVA, Tukey.

metabolism-related genes in skeletal muscle and bone. In skeletal muscle, AZ increased glucose transporter, Glut1, Glut3, and Glut4, gene expression, and led to a tendency towards increase in Glut2 gene expression in mice at both ages (Fig. 8A). Further, in skeletal muscle PGK1 and LDHA expression was increased, while the PGC-1α and PPAR-α expression was unchanged with AZ treatment in young and middle-aged mice (Fig. 8B,C). In bone, AZ treatment increased Glut1 and Glut3 gene expression and led to a tendency towards increase in Glut2 gene expression, while Glut4 was not changed (Fig. 8D). Similarly, PGK1 and PGC1α expression was increased in bone lysates from AZ-treated mice at both ages (Fig. 8E,F). Interestingly, we also found that the mRNA expression of leptin and IGF-1, factors known to alter cell metabolism, were also differentially altered with aging in skeletal muscle and bone tissue lysates (Fig. S4). However, AZ led to similar decreases in leptin levels in both tissues at both ages.

3. Discussion

Inflammation is a complex biological process initiated in many cell types in response to various stimuli, which stimulates the secretion of numerous factors and subsequently mediates processes such as protective immunity, tissue repair and damage resolution [6]. Further, while acute inflammation stimulates repair, chronic-sustained

inflammation leads to progressive damage [21]. Particularly, chronic low-grade inflammation has been associated with numerous age-related degenerative diseases and with related debilitating conditions, such as sarcopenia and osteoporosis [16,23]. Several potential mechanisms of age-associated chronic inflammation have been proposed, including the accumulation senescent cells, impaired mitochondrial function, reduced levels of autophagy, and altered NF-κB signaling [6,21], which are also seen in bone and skeletal muscle with aging [42,43].

Consistently, sustained RAGE signaling, a known regulator of NF-κB, has been shown to contribute to the onset/progression of various aging-related pathologies [16,23]. Particularly, several pieces of evidence have highlighted the potential involvement of elevated RAGE signaling in the onset/progression of bone and muscle pathology in aging [27–29]. However, given the physiological importance of inflammation, whether blocking RAGE can reverse aging-related pathologies, particularly, osteoporosis and sarcopenia, remains unknown.

In this study, we tested the effects of short-term systemic administration of the small-molecule RAGE inhibitor, AZ, on bone and skeletal muscle in aging using a series of *in vitro* and *in vivo* experiments. Overall, our findings provide evidence that short-term pharmacologic RAGE inhibition has effects on bone and muscle metabolism in young and middle-aged mice.

Consistent with previous findings in global genetic RAGE knockout

mice [27,44,45], RAGE inhibition by AZ treatment decreased osteoclast differentiation in vitro. However, *in vivo* AZ administration suppressed bone remodeling and led to a small but significant decrease in BMD in young and middle-aged mice. These findings are consistent with previous studies showing that femoral cancellous bone accrual and architecture were decreased, and femur osteoblast gene (ALP, Cola1, Runx2, and Osterix) expression was lower in 4-month-old RAGE knockout compared to control wildtype mice [46]. Interestingly, despite these cellular changes, bone geometry and strength were maintained. Nevertheless, our findings provide further support for the important physiological role of RAGE signaling in bone. However, opposed to previous findings in RAGE knockout mice, our results suggest that systemic administration of a small-molecule RAGE inhibitor may have both direct and indirect effects in bone cells that differentially regulate bone metabolism.

Particularly, the differential *in vitro* versus *in vivo* effects of AZ on osteoclasts may be due to the increases in cell death and inflammatory cytokine production in osteocytes both *in vitro* and *in vivo*. Hence, despite the direct inhibitory effects of AZ treatment on osteoclasts, the effects of RAGE inhibition in osteocytes may indirectly promote bone resorption. Considering previous reports that NF-κB signaling is required for proper osteoclast function and that AGE-RAGE mediated activation NF-κB signaling induces osteoclastogenesis [36,47] coupled with the known anti-apoptotic effects of NF-κB signaling [48], inhibition of NF-κB signaling may mediate the differential effects of AZ.

Future studies will be designed to examine whether administering a different dose or altering the treatment regimen [intermittent vs chronic], previously seen with other therapeutics, could optimize the beneficial effects of AZ on bone. For example, depending on the mode of administration, intermittent vs chronic, parathyroid hormone (PTH), has anabolic or catabolic actions on the skeleton [49]. Notably, the catabolic actions of PTH have been shown to be mediated through indirect actions on osteoblasts and osteocytes, by modulating RANKL and MCP-1 levels [50–52], both of which were increased by AZ. Further, because the mild skeletal phenotype observed in mice receiving AZ could be due to modest changes in formation and resorption occurring over a short treatment window, future studies will explore the long-term effect of AZ administration.

Previous studies showed that AGEs, HMGB1, APP, and amyloid β are present in bone [53]. However, while the levels of RAGE ligands have been shown to increase with age [15,16], to our knowledge, no study evaluated the levels of these ligands in bone with aging. It is possible that a mouse with increased activation of RAGE, such as the models of diabetes or other inflammatory conditions with increased levels of RAGE ligands, for example, are needed to put in evidence the effect of the RAGE inhibitor in bone.

In contrast to the effects of AZ on bone, we found that treatment reversed the aging-induced alterations in body composition, leading to lower fat and higher lean body mass compared to veh-treated control mice at both ages. These findings are consistent with recent studies demonstrating that RAGE signaling regulates the metabolic and inflammatory response to high fat feeding in mice [54]. In this study, genetic RAGE deficiency and administration of systemic soluble RAGE, a decoy receptor RAGE isoform, reduced fat mass in high fat diet fed mice. Although, despite the beneficial effects of AZ administration on the skeletal muscle of middle-aged mice, AZ had differential effects on skeletal muscles of young animals. Specifically, while several similar positive effects were detected in the tibialis anterior muscle, quadriceps mass was decreased and ubiquitin-mediated protein degradation was increased in young AZ-treated mice.

Nevertheless, consistent with the beneficial effects on lean body mass, we found that AZ treatment reversed the aging-induced decreases in skeletal muscle mass and attenuated several aging-induced changes known to be associated with chronic inflammation, including NF-κB signaling, mitochondrial function and autophagy. Specifically, AZ preserved the expression of known myogenic regulatory factors, such as

myogenin and MyoD, and attenuated ubiquitin-mediated protein degradation in the aged mice. Consistently, it has been suggested that activation of NF-κB post-transcriptionally reduces the cellular levels of MyoD [55]. Further, deletion of the β subunit of the inhibitor of NF-κB kinase, IKKβ, reduces inflammation, leading to improved skeletal muscle strength, maintained mass, and enhanced regeneration [56].

In addition, AGEs induce skeletal muscle atrophy and dysfunction in diabetic mice via RAGE-mediated AMPK-induced downregulation of the Akt pathway [30]. In this study, Atrogin-1 levels were attenuated following RAGE inhibition and consistent with this, Atrogin-1 has been previously shown to directly suppress MyoD expression, inhibiting protein synthesis and inducing aging-related skeletal muscle atrophy [57]. Consistently, reports suggest that the association between Atrogin-1 and skeletal muscle atrophy may be more related to its inhibitory effects on protein synthesis [58,59]. Taken together these pieces of evidence suggest that in middle-aged mice AZ treatment may restore key cellular processes normally involved in the maintenance of skeletal muscle mass by directly inhibiting AGE-RAGE signaling or by downregulating NF-κB signaling in the skeletal muscle.

However, given the increased myotube diameter in C2C12 cultures exposed to serum from middle-aged AZ-treated mice, it is also possible that the observed beneficial effects are due to systemic alterations rather than direct effect of AZ in skeletal muscle. Thus, additional studies are needed to understand the mechanisms underlying the beneficial effects of systemic AZ treatment on skeletal muscle in middle-aged mice. Additionally, whether AZ administration also improves muscle function remains to be elucidated.

Nevertheless, our findings suggest that systemic AZ treatment in middle-aged mice might contribute to reverse the derangements observed in the skeletal muscle primarily by attenuating the aging-associated metabolic defects and by preventing the effects of AGEs and potentially other RAGE ligands. Indeed, our findings that AZ treatment protects against the aging-related decreases in skeletal muscle glucose transporter gene expression, are consistent with reports that AGEs inhibit insulin actions in skeletal muscle and induce interference of glucose uptake [60]. In particular, AGE-RAGE binding induces inflammation, triggering ER-stress and initiating the unfolded protein response (UPR), which subsequently promotes nuclear translocation of NF-κB [61,62]. Further, recent work demonstrated that nuclear NF-κB directly binds and represses Slc2a4 gene transcription, suppressing GLUT4 expression and disrupting glucose uptake [63]. Thus, our findings that aging decreased skeletal muscle GLUT4 gene expression, an effect reversed by AZ administration, suggest that systemic RAGE inhibition reverses the aging-induced alterations in skeletal muscle glucose uptake, potentially by blocking AGE actions on skeletal muscle.

Further, AZ treatment reversed the aging-induced declines in the expression of skeletal muscle glycolytic, but not oxidative metabolism enzymes, which is consistent with reports that NF-κβ activation primarily induces fast-twitch, glycolytic muscle fiber atrophy [64]. However, despite the findings that AZ treatment had similar effects on glucose transporter and glycolytic enzyme gene expression in bone, aging had opposite effects on their expression in bone and skeletal muscle. Altogether, these findings suggest that aging differentially affects glucose uptake and metabolism in the different tissues, which highlights a potential mechanism underlying the differential effects of AZ treatment on bone and skeletal muscle in aging.

In conclusion, our study suggests that short-term pharmacologic RAGE inhibition has distinct effects on bone and muscle metabolism. Thus, while AZ treatment did not attenuate the aging-induced alterations in bone, it did rescue some of the changes in skeletal muscle. In particular, our data points towards a role of RAGE signaling in promoting musculoskeletal derangements associated with aging, thus making it an interesting therapeutic target. Altogether, our findings strongly support that idea that AZ may represent a novel therapeutic option for the treatment of the effects of aging on skeletal muscle.

4. Experimental procedures

4.1. Osteoclastogenesis assay

Non-adherent BMCs (6×10^4 cells/cm^2) were plated on a 96-well plate with α-minimal essential medium (MEM) supplemented with 10% FBS and 1% penicillin/streptomycin (P/S) plus recombinant murine M-CSF (20 ng/ml) and soluble RANKL (80 ng/ml) (PeproTech Inc., Rocky Hill, NJ, USA) with either 100 ng/ml AZ or veh. Media was changed every 2 days for 7 days [65]. Mature osteoclasts (> 3 or more nuclei) were quantified after staining for TRAPase using a commercial kit (Sigma-Aldrich, Saint Louis, MO, USA, cat.#387A). Images were acquired using a Zeiss Axiovert 35 microscope equipped with a digital camera (Carl Zeiss, Thronwood, NY, USA). mRNA was isolated from parallel cultures and gene expression was measured by qPCR (Applied Biosystems, Foster City, CA, USA).

4.2. RNA extraction and qPCR

Total RNA was isolated using TRIzol (Invitrogen, Grand Island, NY, USA), as published [65,66]. Reverse transcription was performed using a high-capacity cDNA kit (Applied Biosystems, Foster City, CA, USA). qPCR was performed using the Gene Expression Assay Mix TaqMan Universal Master Mix with an ABI 7900HT real-time PCR system. The house-keeping gene glyceraldehyde 3-phosphate dehydrogenase (GAPDH) was used. Primers and probes were commercially available (Applied Biosystems, Foster City, CA, USA) or were designed using the Assay Design Center (Roche Applied Science, Indianapolis, IN, USA). Relative expression was calculated using the ΔCt method [67].

4.3. Mice and treatment

4- (young, $n = 10$) and 15-month-old mice (middle-aged, n = 10) C57BL/6 female mice were obtained from National Institute on Aging (NIA) and received daily intraperitoneal injection of veh (1.7% DMSO) or 100 μg/day (young mice) and 110 μg/day (middle-aged mice) of AZ (DC Chemicals, Shanghai, P.R., China, cat.# DC8338), to account for body weight differences, for 28 days. We chose these 2 ages to determine the effect of RAGE inhibition at the age in which the mice reach peak bone mass (4 months of age), and later in life (15 months of age), in which we showed there is already a significant deterioration, without reaching very low levels of bone mass and strength that might be difficult to reverse [68]. Mice were assigned an ID number and the age/treatment were recorded in a database. Investigators performing endpoint measurements were only given the mouse ID. Mice were randomized and assigned to each experimental group based on spinal BMD. Mice (4–5/cage) were fed a regular diet (Envigo, Indianapolis, IN) and water ad libitum, and maintained on a 12 h light/dark cycle. Animals were sacrificed between 3 and 5 h after last injection. All experiments were carried out as planned. No mortality was recorded throughout the experiment, although 2 old mice exhibited signs of infections near the injection sites. In addition, AZ administration induced splenomegaly (Fig. S5), but no other signs of distress were recorded. Young mice received IP injections of calcein (30 mg/kg; Sigma-Aldrich, Saint Louis, MO, USA) and alizarin red (50 mg/kg; Sigma) 7 and 2 days before sacrifice, respectively and aged mice received IP injections of calcein (30 mg/kg; Sigma-Aldrich, Saint Louis, MO, USA) and alizarin red (50 mg/kg; Sigma) 10 and 3 days before sacrifice, respectively, to allow for dynamic histomorphometric measurements [68]. The longer duration between labels in aged mice was done to help facilitate the differentiation of the two labels given the slower bone formation rate.

4.4. Bone histomorphometry

Femora and lumbar vertebrae (L1–L3) were dissected and fixed in 10% neutral buffered formalin as previously published [68]. Static histomorphometric analysis was performed on the cancellous surface of sequential methyl methacrylate embedded lumbar vertebrae sections stained with von Kossa/McNeal [osteoblasts] and TRAPase/Toludine blue [osteoclasts]. Additionally, osteoclasts were quantified on the endocortical surface paraffin embedded TRAPase/Toludine blue stained femur cortical bone cross-sections. Dynamic histomorphometric measurements were performed in unstained plastic embedded femoral mid-diaphysis and lumbar vertebrae bone sections [66]. Histomorphometric analysis was performed using OsteoMeasure high-resolution digital video system (OsteoMetrics Inc., Decatur, GA, USA) [68]. The terminology and units used are those recommended by the Histomorphometry Nomenclature Committee of the American Society for Bone and Mineral Research [69].

4.5. Serum biochemistry

Blood was collected by cheek bleeding after 3 h of fasting. Plasma was separated, aliquoted, and stored at −80 °C [70]. N-terminal propeptide of type I procollagen (P1NP) (Immunodiagnostic Systems Inc., Fountain Hill, AZ, USA, cat.#AC-33F1) and C-telopeptide fragments (CTX) (RatLaps, Immunodiagnostic Systems Inc., Fountain Hill, AZ, USA, cat.#AC-06F1) were measured as previously published [68].

4.6. Osteoblast mineralization assay

Adherent-BMCs were cultured for 10 days in α-MEM supplemented with 10% FBS and 1% penicillin/streptomycin in the presence of 50 μM ascorbic acid and 10 mM β-glycerol phosphate, as previously described [71]. Cells were fixed with 3.7% paraformaldehyde in PBS for 1 h, rinsed twice with distilled water, and stained for 10 min with 40 mM Alizarin Red S (pH 4.2) at room temperature under shaking. Cells were then washed 5 times with water, followed by a 15 min-wash with PBS. Alizarin Red S was extracted by adding 1% cetylpyridinium chloride for 15 min at room temperature with shaking. OD was measured at 490 nm.

4.7. Apoptosis

Osteocyte apoptosis was detected in paraffin-embedded femur cross-sections using previously published protocols [72]. Briefly, femora were deparaffinized, treated with 3% H_2O_2 to inhibit endogenous peroxidase activity, blocked and then incubated with rabbit monoclonal anti-active caspase-3 antibody (1:75; Thermo Fisher Scientific In., Rockford, IL, USA, cat.#PA5-23921) [73]. Sections were then incubated with anti-rabbit biotinylated secondary antibody followed by avidin conjugated peroxidase (Vectastain Elite ABC Kit; Vector Laboratories Inc., Burlingame, CA, USA). Color was developed with a diaminobenzidine substrate chromogen system (Acros Organics, New Jersey, USA). Cells expressing the protein of interest are stained in brown, whereas negative cells are green-blue. Nonimmune IgG was used as negative control.

4.8. Ex vivo bone organ cultures

Long bones were isolated from 4- and 16-month-old female C57BL/6 mice and BMCs were flushed out with α-MEM. Osteocyte-enriched marrow-flushed long bones were cultured ex vivo in α-MEM supplemented with 10% FBS and 1% P/S with veh or AZ (100 ng/ml) and cultured for 24 h. Following treatment, bones were collected, frozen in liquid nitrogen, and stored at −80 °C. Gene expression was measured by qPCR (Applied Biosystems, Foster City, CA, USA).

4.9. Bone mineral density (BMD) and body composition (fat and lean mass) by dual energy x-ray absorptiometry (DXA)

Bone mineral density (BMD) and body composition were measured monthly by dual X-ray absorptiometry (DXA) using a PIXImus

densitometer (G.E. Medical Systems, Lunar Division, Madison, WI, USA) [74]. BMD measurements included total BMD (excluding the head and tail), entire femur (femoral BMD) and L1–L6 vertebra (spinal BMD) [68]. Body composition included body weight, fat mass, and lean mass. Calibration was performed before scanning with a standard phantom, as recommended by the manufacturer.

4.10. Micro-computed tomography (μCT) analysis

Femora and L4 vertebrae were dissected, wrapped in saline-soaked gauze and frozen at −20 °C [68]. Vertebra and femora, 6 bones per scan, were scanned using a 65 kV source, 0.5 mm Al filter, 0.7 degree rotation and two-image averaging with an isotropic voxel size of 9 μm using a SkyScan 1176 system (SkyScan, Kontich, Belgium). Scans were reconstructed and analyzed using manufacturer software. Nomenclature is reported in accordance with the guidelines for μCT [75].

4.11. Biomechanical testing

Femoral three-point bending testing was performed following previously published protocols [68]. Structural mechanical properties, ultimate load, stiffness, displacement and work were determined from the load–deformation curves using standard definitions while material-level estimations of properties were calculated using standard equations. Cross-sectional moment of inertia and anterior–posterior diameter were determined by μCT and were used to calculate material-level properties, as previously described [68].

4.12. Muscle weight

Skeletal muscles gastrocnemius, tibialis anterior, quadriceps and soleus, were harvested and weighed immediately following dissection. Muscle weight was corrected by total body weight and reported as the percentage of muscle per body weight. After weighing, muscles were snap frozen and store at −80 °C until used for gene expression analysis.

4.13. Muscle histology and morphometric analysis

The forearms of mice were removed and fixed in 10% neutral buffered formalin. Forearms were cross-sectioned, demineralized, and embedded in paraffin and then sectioned on a microtome. Tissue morphology was assessed on 4 μm–thick cross-sections of muscles sections stained with hematoxylin and eosin (H&E) dye. Myofiber cross-sectional area (CSA) was analyzed on H&*E*-stained forearm muscle section images using image J analysis software and tablet input device [76].

4.14. C2C12 cell culture and myotube diameter measurement

C2C12 myoblasts (ATCC, Manassas, VA) were grown and seeded onto 12-well plates (7500 cells/cm^2). The cells were then exposed to DMEM supplemented with horse serum for five days, then subsequently treated for 48 h with 5% serum from young or aged animals treated with veh or AZ. Myotubes were fixed using chilled acetone/methanol (1:1) and washed with PBS, stained using a primary antibody against myosin heavy chain (#MF-20, Developmental Studies Hybridoma Bank, Iowa City, IA) overnight at 4 °C, then stained with Alexaflour 594-labeled secondary antibody (Invitrogen, Grand Island, NY) at room temperature for one hour. Myotubes were imaged using an Axio Observer.Z1 motorized microscope (Zeiss, Oberchoken, Germany). Average myotube diameter was measured per field of view using Image J analysis software [77] and a Cintiq pen tablet input device (Wacom, Vancouver, WA).

4.15. Western blot analysis

Ubiquitin-conjugated protein levels were evaluated in protein lysates isolated from the quadriceps of young and aged veh- and AZ-treated mice. Protein lysates were separated on 10% SDS–PAGE gels (BioRad) and electrotransferred to nitrocellulose membranes (Millipore, Billerica, MA, USA). Membranes were then incubated in blocking solution (SEABlock) for 60 min and probed with primary antibodies diluted 1:1000 in SeaBLOCK +0.2% Tween against a monoclonal anti-Ubiqutin (#3933, Cell Signaling Technologies, Danvers, MA) overnight at 4 °C, followed by corresponding secondary fluorescent antibodies diluted 1:10,000 in SEABlock +0.2% Tween for 1 h at room temperature. After rinsing with PBS-T, the membranes were developed using LICOR imaging. Bands were detected using an Odyssey Infrared Imaging System (LI-COR Biosciences, Lincoln, NE, USA), and their intensity was quantified using ImageJ.

4.16. Statistical analysis

Data were analyzed by using SigmaPlot (Systat Software Inc., San Jose, CA, USA). All values are reported as the mean ± standard deviation. Differences were evaluated either by two-way ANOVA with post-hoc analysis using Tukey Method or by Student's *t*-test, as appropriate. Differences were considered significant when $p < 0.05$.

Author contributions

Study design performed by HMD and LIP. Data acquisition performed by HMD, ALE, SV, and PD. Advice on μCT analysis and biomechanical testing was provided by MWA and MRA. AB provided advice for experiments in which measurements were performed on skeletal muscle. Data analysis/interpretation performed by HMD, ALE, AB and LIP. Manuscript written by HMD and LIP. All authors revised the manuscript and approved the final version.

Acknowledgements

Appendix A. Supplementary data

Supplementary data to this article can be found online at https://doi.org/10.1016/j.bone.2019.04.012.

References

[1] C. Franceschi, P. Garagnani, C. Morsiani, M. Conte, A. Santoro, A. Grignolio, S. Salvioli, The continuum of aging and age-related diseases: common mechanisms but different rates, Front Med (Lausanne) 5 (2018) 61, , https://doi.org/10.3389/fmed.2018.00061.

[2] S. Khosla, J.N. Farr, J.L. Kirkland, Inhibiting cellular senescence: a new therapeutic paradigm for age-related osteoporosis, J. Clin. Endocrinol. Metab. 103 (4) (2018) 1282–1290, https://doi.org/10.1210/jc.2017-02694.

[3] F. Rodier, D. Zhou, G. Ferbeyre, Cellular senescence, geroscience, cancer and beyond, Aging (Albany NY) 10 (9) (2018) 2233–2242, https://doi.org/10.18632/aging.101546.

[4] D.R. Seals, J.N. Justice, T.J. LaRocca, Physiological geroscience: targeting function to increase healthspan and achieve optimal longevity, J. Physiol. 594 (8) (2016) 2001–2024, https://doi.org/10.1113/jphysiol.2014.282665.

[5] Y. Gerakis, C. Hetz, A decay of the adaptive capacity of the unfolded protein response exacerbates Alzheimer's disease, Neurobiol. Aging 63 (2018) 162–164, https://doi.org/10.1016/j.neurobiolaging.2017.09.012.

[6] T.K. Howcroft, J. Campisi, G.B. Louis, M.T. Smith, B. Wise, T. Wyss-Coray, F. Sierra, The role of inflammation in age-related disease, Aging (Albany NY) 5 (1) (2013)

84–93, https://doi.org/10.18632/aging.100531.

[7] B. Abrahamsen, T. van Staa, R. Ariely, M. Olson, C. Cooper, Excess mortality following hip fracture: a systematic epidemiological review, Osteoporos. Int. 20 (10) (2009) 1633–1650, https://doi.org/10.1007/s00198-009-0920-3.

[8] S. Fischer, K.A. Kapinos, A. Mulcahy, L. Pinto, O. Hayden, R. Barron, Estimating the long-term functional burden of osteoporosis-related fractures, Osteoporos. Int. 28 (10) (2017) 2843–2851, https://doi.org/10.1007/s00198-017-4110-4.

[9] A.S. Sousa, R.S. Guerra, I. Fonseca, F. Pichel, S. Ferreira, T.F. Amaral, Financial impact of sarcopenia on hospitalization costs, Eur. J. Clin. Nutr. 70 (9) (2016) 1046–1051, https://doi.org/10.1038/ejcn.2016.73.

[10] A. Tournadre, G. Vial, F. Capel, M. Soubrier, Y. Boirie, Sarcopenia, Joint Bone Spine. (2018), https://doi.org/10.1016/j.jbspin.2018.08.001.

[11] K.H. Collins, W. Herzog, G.Z. MacDonald, R.A. Reimer, J.L. Rios, I.C. Smith, D.A. Hart, Obesity, metabolic syndrome, and musculoskeletal disease: common inflammatory pathways suggest a central role for loss of muscle integrity, Front. Physiol. 9 (2018) 112, , https://doi.org/10.3389/fphys.2018.00112.

[12] G. Karsenty, P. Mera, Molecular bases of the crosstalk between bone and muscle, Bone 115 (2018) 43–49, https://doi.org/10.1016/j.bone.2017.04.006.

[13] J.Y. Reginster, C. Beaudart, F. Buckinx, O. Bruyere, Osteoporosis and sarcopenia: two diseases or one? Curr Opin Clin Nutr Metab Care 19 (1) (2016) 31–36, https://doi.org/10.1097/MCO.0000000000000230.

[14] D. Agostini, S. Zeppa Donati, F. Lucertini, G. Annibalini, M. Gervasi, C. Ferri Marini, P. Sestili, Muscle and bone health in postmenopausal women: role of protein and vitamin D supplementation combined with exercise training, Nutrients 10 (8) (2018), https://doi.org/10.3390/nu10081103.

[15] D.S. Amarasekara, J. Yu, J. Rho, Bone loss triggered by the cytokine network in inflammatory autoimmune diseases, J Immunol Res 2015 (2015) 832127, , https://doi.org/10.1155/2015/832127.

[16] R. Ramasamy, A. Shekhtman, A.M. Schmidt, The multiple faces of RAGE—opportunities for therapeutic intervention in aging and chronic disease, Expert Opin. Ther. Targets 20 (4) (2016) 431–446, https://doi.org/10.1517/14728222.2016.1111873.

[17] M.T. Heneka, M.J. Carson, K.J. El, G.E. Landreth, F. Brosseron, D.L. Feinstein, ... M.P. Kummer, Neuroinflammation in Alzheimer's disease, Lancet Neurol. 14 (4) (2015) 388–405 doi:S1474–4422(15)70016–5 [pii] https://doi.org/10.1016/S1474-4422(15)70016-5.

[18] J.P. Bidwell, J. Yang, A.G. Robling, Is HMGB1 an osteocyte alarmin? J. Cell. Biochem. 103 (6) (2008) 1671–1680, https://doi.org/10.1002/jcb.21572 [doi].

[19] G. Karsenty, P. Mera, Molecular bases of the crosstalk between bone and muscle, Bone. (2017), https://doi.org/10.1016/j.bone.2017.04.006.

[20] U. Andersson, H. Yang, H. Harris, Extracellular HMGB1 as a therapeutic target in inflammatory diseases, Expert Opin. Ther. Targets 22 (3) (2018) 263–277, https://doi.org/10.1080/14728222.2018.1439924.

[21] B. Fougere, E. Boulanger, F. Nourhashemi, S. Guyonnet, M. Cesari, Chronic inflammation: accelerator of biological aging, J. Gerontol. A Biol. Sci. Med. Sci. 72 (9) (2017) 1218–1225, https://doi.org/10.1093/gerona/glw240.

[22] A. Picca, R. Calvani, E. Manes-Gravina, L. Spaziani, F. Landi, R. Bernabei, E. Marzetti, Bone-muscle crosstalk: unraveling new therapeutic targets for osteoporosis, Curr. Pharm. Des. 23 (41) (2017) 6256–6263, https://doi.org/10.2174/1381612823666170526112300.

[23] A.L. Cardoso, A. Fernandes, J.A. Aguilar-Pimentel, M.H. de Angelis, J.R. Guedes, M.A. Brito, ... A.U. Trendelenburg, Towards frailty biomarkers: candidates from genes and pathways regulated in aging and age-related diseases, Ageing Res. Rev. (2018), https://doi.org/10.1016/j.arr.2018.07.004.

[24] E.J. Lee, J.H. Park, Receptor for advanced glycation endproducts (RAGE), its ligands, and soluble RAGE: potential biomarkers for diagnosis and therapeutic targets for human renal diseases, Genomics Inform 11 (4) (2013) 224–229, https://doi.org/10.5808/GI.2013.11.4.224 [doi].

[25] G. Sorci, F. Riuzzi, I. Giambanco, R. Donato, RAGE in tissue homeostasis, repair and regeneration, Biochim. Biophys. Acta 1833 (1) (2013) 101–109, https://doi.org/10.1016/j.bbamcr.2012.10.021.

[26] A.M. Schmidt, Soluble RAGEs - prospects for treating & tracking metabolic and inflammatory disease, Vasc. Pharmacol. 72 (2015) 1–8, https://doi.org/10.1016/j.vph.2015.06.011.

[27] K.H. Ding, Z.Z. Wang, M.W. Hamrick, Z.B. Deng, L. Zhou, B. Kang, Q.S. Mi, Disordered osteoclast formation in RAGE-deficient mouse establishes an essential role for RAGE in diabetes related bone loss, Biochem. Biophys. Res. Commun. 340 (4) (2006) 1091–1097, https://doi.org/10.1016/j.bbrc.2005.12.107.

[28] E. Lalla, I.B. Lamster, M. Feit, L. Huang, A. Spessot, W. Qu, A.M. Schmidt, Blockade of RAGE suppresses periodontitis-associated bone loss in diabetic mice, J. Clin. Invest. 105 (8) (2000) 1117–1124, https://doi.org/10.1172/JCI8942.

[29] T. Egawa, S. Tsuda, A. Goto, Y. Ohno, S. Yokoyama, K. Goto, T. Hayashi, Potential involvement of dietary advanced glycation end products in impairment of skeletal muscle growth and muscle contractile function in mice, Br. J. Nutr. 117 (1) (2017) 21–29, https://doi.org/10.1017/S0007114516004591.

[30] C.Y. Chiu, R.S. Yang, M.L. Sheu, D.C. Chan, T.H. Yang, K.S. Tsai, S.H. Liu, Advanced glycation end-products induce skeletal muscle atrophy and dysfunction in diabetic mice via a RAGE-mediated, AMPK-down-regulated, Akt pathway, J. Pathol. 238 (3) (2016) 470–482, https://doi.org/10.1002/path.4674.

[31] C. Tubaro, C. Arcuri, I. Giambanco, R. Donato, S100B protein in myoblasts modulates myogenic differentiation via NF-kappaB-dependent inhibition of MyoD expression, J. Cell. Physiol. 223 (1) (2010) 270–282, https://doi.org/10.1002/jcp.22035.

[32] S. Bongarzone, V. Savickas, F. Luzi, A.D. Gee, Targeting the receptor for advanced glycation endproducts (RAGE): a medicinal chemistry perspective, J. Med. Chem. 60 (17) (2017) 7213–7232, https://doi.org/10.1021/acs.jmedchem.7b00058.

[33] F. Panza, D. Seripa, V. Solfrizzi, B.P. Imbimbo, M. Lozupone, A. Leo, G. Logroscino, Emerging drugs to reduce abnormal beta-amyloid protein in Alzheimer's disease patients. *Expert. Opin. Emerg,* Drugs 21 (4) (2016) 377–391, https://doi.org/10.1080/14728214.2016.1241232 [doi].

[34] D. Walker, L.F. Lue, G. Paul, A. Patel, M.N. Sabbagh, Receptor for advanced glycation endproduct modulators: a new therapeutic target in Alzheimer's disease, Expert Opin. Investig. Drugs 24 (3) (2015) 393–399, https://doi.org/10.1517/13543784.2015.1001490.

[35] JAX® Mice, C. R. S. (2017). Aged C57BL/6J mice for research studies: Considerations, applications and best practices.

[36] Z. Zhou, W.C. Xiong, RAGE and its ligands in bone metabolism, Front Biosci (Schol Ed) 3 (2011) 768–776.

[37] Jilka, R. L., & O'Brien, C. A. (2016). The role of osteocytes in age-related bone loss. *Curr. Osteoporos. Rep, 14*(1), 16–25. doi:10.1007/s11914-016-0297-0 [doi];https://doi.org/10.1007/s11914-016-0297-0 [pii].

[38] M. Almeida, L. Han, M. Martin-Millan, L.I. Plotkin, S.A. Stewart, P.K. Roberson, S.C. Manolagas, Skeletal involution by age-associated oxidative stress and its acceleration by loss of sex steroids, J. Biol. Chem. 282 (37) (2007) 27285–27297.

[39] S.H. Lecker, R.T. Jagoe, A. Gilbert, M. Gomes, V. Baracos, J. Bailey, A.L. Goldberg, Multiple types of skeletal muscle atrophy involve a common program of changes in gene expression, FASEB J. 18 (1) (2004) 39–51, https://doi.org/10.1096/fj.03-0610com.

[40] M. Sandri, C. Sandri, A. Gilbert, C. Skurk, E. Calabria, A. Picard, A.L. Goldberg, Foxo transcription factors induce the atrophy-related ubiquitin ligase atrogin-1 and cause skeletal muscle atrophy, Cell 117 (3) (2004) 399–412.

[41] A.Y. Sato, D. Richardson, M. Cregor, H.M. Davis, E.D. Au, K. McAndrews, T. Bellido, Glucocorticoids induce bone and muscle atrophy by tissue-specific mechanisms upstream of E3 ubiquitin ligases, Endocrinology 158 (3) (2017) 664–677.

[42] P. Bonaldo, M. Sandri, Cellular and molecular mechanisms of muscle atrophy, Dis. Model. Mech. 6 (1) (2013) 25–39.

[43] T.H. Lin, J. Pajarinen, L. Lu, A. Nabeshima, L.A. Cordova, Z. Yao, S.B. Goodman, NF-kappaB as a therapeutic target in inflammatory-associated bone diseases, Adv Protein Chem Struct Biol 107 (2017) 117–154, https://doi.org/10.1016/bs.apcsb.2016.11.002.

[44] K. Charoonpatrapong, R. Shah, A.G. Robling, M. Alvarez, D.W. Clapp, S. Chen, J.P. Bidwell, HMGB1 expression and release by bone cells, J. Cell. Physiol. 207 (2) (2006) 480–490, https://doi.org/10.1002/jcp.20577.

[45] Z. Zhou, D. Immel, C.X. Xi, A. Bierhaus, X. Feng, L. Mei, W.C. Xiong, Regulation of osteoclast function and bone mass by RAGE, J. Exp. Med. 203 (4) (2006) 1067–1080.

[46] B.K. Philip, P.J. Childress, A.G. Robling, A. Heller, P.P. Nawroth, A. Bierhaus, J.P. Bidwell, RAGE supports parathyroid hormone-induced gains in femoral trabecular bone, Am. J. Physiol. Endocrinol. Metab. 298 (3) (2010) E714–E725.

[47] B.F. Boyce, Y. Xiu, J. Li, L. Xing, Z. Yao, NF-kappaB-mediated regulation of osteoclastogenesis, Endocrinol Metab (Seoul) 30 (1) (2015) 35–44, https://doi.org/10.3803/EnM.2015.30.1.35.

[48] D.V. Novack, Role of NF-kappaB in the skeleton, Cell Res. 21 (1) (2011) 169–182.

[49] Silva, B. C., & Bilezikian, J. P. (2015). Parathyroid hormone: anabolic and catabolic actions on the skeleton. *Curr. Opin. Pharmacol, 22*, 41–50. doi:S1471–4892(15) 00035–1 [pii];https://doi.org/10.1016/j.coph.2015.03.005 [doi].

[50] X. Li, L. Qin, M. Bergenstock, L.M. Bevelock, D.V. Novack, N.C. Partridge, Parathyroid hormone stimulates osteoblastic expression of MCP-1 to recruit and increase the fusion of pre/osteoclasts, J. Biol. Chem. 282 (45) (2007) 33098–33106.

[51] R. Murrills, Parathyroid hormone and bone cells, Clinical Reviews in Bone & Mineral Metabolism 4 (4) (2008) 233–257.

[52] Wein, M. N., & Kronenberg, H. M. (2018). Regulation of bone remodeling by parathyroid hormone. *Cold Spring Harb. Perspect. Med, 8*(8), pii: a031237. doi:csh-perspect.a031237 [pii];https://doi.org/10.1101/cshperspect.a031237 [doi].

[53] L.I. Plotkin, A.L. Essex, H.M. Davis, RAGE signaling in skeletal biology, Curr Osteoporos Rep. (2019), https://doi.org/10.1007/s11914-019-00499-w.

[54] F. Song, C. Hurtado del Pozo, R. Rosario, Y.S. Zou, R. Ananthakrishnan, X. Xu, A.M. Schmidt, RAGE regulates the metabolic and inflammatory response to high-fat feeding in mice, Diabetes 63 (6) (2014) 1948–1965, https://doi.org/10.2337/db13-1636.

[55] H. Li, S. Malhotra, A. Kumar, Nuclear factor-kappa B signaling in skeletal muscle atrophy, J Mol Med (Berl) 86 (10) (2008) 1113–1126, https://doi.org/10.1007/s00109-008-0373-8.

[56] D. Van Gammeren, J.S. Damrauer, R.W. Jackman, S.C. Kandarian, The IkappaB kinases IKKalpha and IKKbeta are necessary and sufficient for skeletal muscle atrophy, FASEB J. 23 (2) (2009) 362–370, https://doi.org/10.1096/fj.08-114249.

[57] A. Fanzani, V.M. Conraads, F. Penna, W. Martinet, Molecular and cellular mechanisms of skeletal muscle atrophy: an update, J. Cachexia. Sarcopenia Muscle 3 (3) (2012) 163–179, https://doi.org/10.1007/s13539-012-0074-6.

[58] T.J. McLoughlin, S.M. Smith, A.D. DeLong, H. Wang, T.G. Unterman, K.A. Esser, FoxO1 induces apoptosis in skeletal myotubes in a DNA-binding-dependent manner, Am J Physiol Cell Physiol 297 (3) (2009) C548–C555, https://doi.org/10.1152/ajpcell.00502.2008.

[59] S.M. Senf, S.L. Dodd, A.R. Judge, FOXO signaling is required for disuse muscle atrophy and is directly regulated by Hsp70, Am. J. Physiol Cell Physiol 298 (1) (2010) C38–C45.

[60] R. Koopman, C.H. Ly, J.G. Ryall, A metabolic link to skeletal muscle wasting and regeneration, Front. Physiol. 5 (2014) 32, , https://doi.org/10.3389/fphys.2014.00032.

[61] T. Anelli, R. Sitia, Protein quality control in the early secretory pathway, EMBO J. 27 (2) (2008) 315–327, https://doi.org/10.1038/sj.emboj.7601974.

[62] C. Piperi, C. Adamopoulos, G. Dalagiorgou, E. Diamanti-Kandarakis,

A.G. Papavassiliou, Crosstalk between advanced glycation and endoplasmic reticulum stress: emerging therapeutic targeting for metabolic diseases, J. Clin. Endocrinol. Metab. 97 (7) (2012) 2231–2242, https://doi.org/10.1210/jc.2011-3408.

[63] D.T. Furuya, E.A. Neri, A.C. Poletto, G.F. Anhe, H.S. Freitas, R.S. Campello, U.F. Machado, Identification of nuclear factor-kappaB sites in the Slc2a4 gene promoter, Mol. Cell. Endocrinol. 370 (1–2) (2013) 87–95, https://doi.org/10.1016/j.mce.2013.01.019.

[64] Y. Wang, J.E. Pessin, Mechanisms for fiber-type specificity of skeletal muscle atrophy, Curr Opin Clin Nutr Metab Care 16 (3) (2013) 243–250, https://doi.org/10.1097/MCO.0b013e328360272d.

[65] H.M. Davis, R. Pacheco-Costa, E.G. Atkinson, L.R. Brun, A.R. Gortazar, J. Harris, L.I. Plotkin, Disruption of the Cx43/miR21 pathway leads to osteocyte apoptosis and increased osteoclastogenesis with aging, Aging Cell 16 (3) (2017) 551–563.

[66] R. Pacheco-Costa, I. Hassan, R.D. Reginato, H.M. Davis, A. Bruzzaniti, M.R. Allen, L.I. Plotkin, High bone mass in mice lacking Cx37 due to defective osteoclast differentiation, J. Biol. Chem. 289 (12) (2014) 8508–8520.

[67] K.J. Livak, T.D. Schmittgen, Analysis of relative gene expression data using real-time quantitative PCR and the 2^{-DDC_T} method, Methods 25 (4) (2001) 402–408.

[68] H.M. Davis, M.W. Aref, A. Aguilar-Perez, R. Pacheco-Costa, K. Allen, S. Valdez, L.I. Plotkin, Cx43 overexpression in osteocytes prevents osteocyte apoptosis and preserves cortical bone quality in aging mice, JBMR Plus (2018), https://doi.org/10.1002/jbm4.10035.

[69] D.W. Dempster, J.E. Compston, M.K. Drezner, F.H. Glorieux, J.A. Kanis, H. Malluche, A.M. Parfitt, Standardized nomenclature, symbols, and units for bone histomorphometry: a 2012 update of the report of the ASBMR Histomorphometry Nomenclature Committee, J. Bone Miner. Res. 28 (1) (2013) 2–17.

[70] R. Pacheco-Costa, H.M. Davis, C. Sorenson, M.C. Hon, I. Hassan, R.D. Reginato, L.I. Plotkin, Defective cancellous bone structure and abnormal response to PTH in cortical bone of mice lacking Cx43 cytoplasmic C-terminus domain, Bone 81 (2015) 632–643.

[71] S. Posritong, J.M. Hong, P.P. Eleniste, P.W. McIntyre, J.L. Wu, E.R. Himes, A. Bruzzaniti, Pyk2 deficiency potentiates osteoblast differentiation and mineralizing activity in response to estrogen or raloxifene, Mol. Cell. Endocrinol. 474 (2018) 35–47, https://doi.org/10.1016/j.mce.2018.02.005.

[72] N. Bivi, K.W. Condon, M.R. Allen, N. Farlow, G. Passeri, L. Brun, L.I. Plotkin, Cell autonomous requirement of connexin 43 for osteocyte survival: consequences for endocortical resorption and periosteal bone formation, J. Bone Min. Res 27 (2) (2012) 374–389.

[73] J. Delgado-Calle, J. Anderson, M.D. Cregor, M. Hiasa, J.M. Chirgwin, N. Carlesso, ... T. Bellido, Bidirectional Notch signaling and osteocyte-derived factors in the bone marrow microenvironment promote tumor cell proliferation and bone destruction in multiple myeloma, Cancer Res. 76 (5) (2016) 1089–1100 doi:0008–5472.CAN-15-1703 [pii];https://doi.org/10.1158/0008-5472.CAN-15-1703 [doi].

[74] Y. Zhang, E.M. Paul, V. Sathyendra, A. Davidson, S. Bronson, S. Srinivasan, H.J. Donahue, Enhanced osteoclastic resorption and responsiveness to mechanical load in gap junction deficient bone, PLoS One 6 (8) (2011) e23516.

[75] M.L. Bouxsein, S.K. Boyd, B.A. Christiansen, R.E. Guldberg, K.J. Jepsen, R. Muller, Guidelines for assessment of bone microstructure in rodents using micro-computed tomography, J. Bone Miner. Res. 25 (7) (2010) 1468–1486.

[76] Bonetto, A., Rupert, J. E., Barreto, R., & Zimmers, T. A. (2016). The colon-26 carcinoma tumor-bearing mouse as a model for the study of cancer cachexia. *J. Vis. Exp* (117). doi:https://doi.org/10.3791/54893 [doi].

[77] C.A. Schneider, W.S. Rasband, K.W. Eliceiri, NIH image to ImageJ: 25 years of image analysis, Nat. Methods 9 (7) (2012) 671–675.

[78] D. Galasko, J. Bell, J.Y. Mancuso, J.W. Kupiec, M.N. Sabbagh, C. van Dyck, ... Alzheimer's Disease Cooperative, S, Clinical trial of an inhibitor of RAGE-Abeta interactions in Alzheimer disease, Neurology 82 (17) (2014) 1536–1542, https://doi.org/10.1212/WNL.0000000000000364.